Algorithmic design of self-folding polyhedra

Shivendra Pandey[a], Margaret Ewing[b], Andrew Kunas[c], Nghi Nguyen[d], David H. Gracias[a,e,1], and Govind Menon[f,1]

[a]Department of Chemical and Biomolecular Engineering, The Johns Hopkins University, Baltimore, MD 21218; [b]School of Mathematics, University of Minnesota, Minneapolis, MN 55455; [c]Department of Computer Science, Brown University, Providence, RI 02912; [d]Department of Mathematics and Statistics, University of Massachusetts, Amherst, MA 01003; [e]Department of Chemistry, The Johns Hopkins University, Baltimore, MD 21218; and [f]Division of Applied Mathematics, Brown University, Providence, RI 02906

Edited by Ken A. Dill, Stony Brook University, Stony Brook, NY, and approved October 13, 2011 (received for review July 6, 2011)

Self-assembly has emerged as a paradigm for highly parallel fabrication of complex three-dimensional structures. However, there are few principles that guide a priori design, yield, and defect tolerance of self-assembling structures. We examine with experiment and theory the geometric principles that underlie self-folding of submillimeter-scale higher polyhedra from two-dimensional nets. In particular, we computationally search for nets within a large set of possibilities and then test these nets experimentally. Our main findings are that (*i*) compactness is a simple and effective design principle for maximizing the yield of self-folding polyhedra; and (*ii*) shortest paths from 2D nets to 3D polyhedra in the configuration space are important for rationalizing experimentally observed folding pathways. Our work provides a model problem amenable to experimental and theoretical analysis of design principles and pathways in self-assembly.

microfabrication | origami | programmable matter | viral capsid

Nature uses hierarchical assembly to construct essential biomolecules such as proteins and nucleic acids and biological containers such as viral capsids. Our increased understanding of biological systems has inspired several synthetic methods of self-assembly (1). Conversely, part of the promise of synthetic self-assembly has been that it may yield essential insights into the formation of biological structure. In order to realize these ambitions, it is necessary to develop model experimental systems and theoretical analyses that make precise the analogies between natural and synthetic self-assembly. Abstraction of the essentials of complex biochemical processes is an important step in this process, and perhaps the simplest abstraction is of the geometric form of a biological structure. Two such abstractions are the Caspar–Klug (CK) theory of viral structure (2) and hydrophobic-polar (HP) lattice models for protein folding (3). The consequences of geometry alone can be striking in such models: The CK theory provides a valuable classification of virus shapes by T number, and much of the detailed architecture of compact proteins such as helices, and antiparallel and parallel sheets emerges from purely steric restrictions on long chain molecules (4). Building such geometric models is, of course, part of a long tradition in biochemistry. What is now striking is the ability to build basic geometric structures such as polyhedra in laboratory self-assembly experiments using molecules such as DNA (5–8) or 100-nm to 1-mm scale lithographically interconnected panels (9). In addition to the intellectual value of such experiments, many of the self-assembled structures realized cannot be fabricated by alternate methods, and they are of technological relevance in optics, electronics, and medicine. In order to translate these self-assembly processes from the laboratory to a manufacturing setting, there is a need to uncover rules that govern yield and defect tolerance. Several experiments, in combination with a growing body of theory, point the way to a future of algorithmic design of biomimetic devices and materials of increasing complexity (10–16).

Our focus in this work is on the role of discrete geometry in self-assembly. We present an experimental and theoretical study of surface-tension driven self-folding of the dodecahedron, icosahedron, and truncated octahedron starting from a two-dimensional template called a net. In geometry, a net is an unfolding of the polyhedron that consists of a single, simply connected, nonoverlapping polygon made up of faces of the polyhedron attached at edges (17, chap. 21). The polyhedron is constructed by folding the net at the edges according to prescribed rules. In our experiments, the nets are realized as patterned panels of side length 300 μm, connected by solder hinges. We study how the choice of initial net determines the folding pathway and yield for these polyhedra. A combinatorial explosion in the set of nets makes this study challenging. Our main finding is that compactness is a simple and effective design principle to maximize the yield of self-folding of polyhedra. We also find that shortest paths between 2D nets and the 3D polyhedron in a discrete model of the configuration space of foldings are a useful idealization of experimentally observed folding pathways. We comment on common themes with other self-assembly models at the end of this article.

Design Criterion for Synthesis by Self-Folding

Nets and Self-Folding Polyhedra. Nets have traditionally been used to build models of polyhedra from a stiff material such as cardboard. They first appear explicitly in Dürer's work in the 15th century (18) and have been used to build a complete set of Archimedean and Platonic solids (19, 20). Despite their importance in classical geometry, a systematic investigation of nets is quite recent and several basic questions are poorly understood (17, chap. 21–23). It is not known if every convex polyhedron has a net (21), nor are there systematic estimates of the number of nets for a given polyhedron, though the number is known for Platonic solids (22). The tetrahedron has two nets, the cube and octahedron have 11 nets each, and the dodecahedron and icosahedron have 43,380 nets each. (Strictly speaking, the calculation of ref. 22 allows *overlapping* nets for the dodecahedron and icosahedron, but we tabulated all 43,380 nets and found no overlap; this was independently verified in ref. 23.) We have also estimated that the truncated octahedron has approximately 2.3 million nets. Such a combinatorial explosion creates an interesting conundrum for engineering design: What criteria determine self-folding with high yield? How do we search efficiently for the "best" net within such a large set?

In our experiments, nets are used as templates for the surface-tension-driven self-folding of polyhedra on the submillimeter scale. The nets are made up of polygonal panels patterned with hinges (Fig. 1) and are fabricated using wafer scale processes such as photolithography, wet etching, and electrodeposition, as described in detail elsewhere (24). Here, we utilized metallic hinges (lead-tin solder) and panels (nickel), but it is noteworthy that elsewhere we have shown that polyhedra can be self-assembled with polymeric panels and hinges (25), suggesting that this self-

Author contributions: D.H.G. and G.M. designed research; S.P., M.E., A.K., N.N., D.H.G., and G.M. performed research; S.P., D.H.G., and G.M. analyzed data; and D.H.G. and G.M. wrote the paper.

The authors declare no conflict of interest.

This article is a PNAS Direct Submission.

[1]To whom correspondence may be addressed. E-mail: menon@dam.brown.edu or dgracias@jhu.edu.

This article contains supporting information online at www.pnas.org/lookup/suppl/doi:10.1073/pnas.1110857108/-/DCSupplemental.

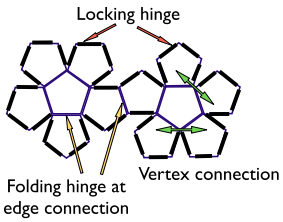

Fig. 1. Schematic diagram of net geometry in experiments. Folding hinges melt and cause panels to rotate. Locking hinges meet and fuse when panels linked at the vertex connection have rotated through approximately the dihedral angle about a folding hinge.

assembly paradigm would apply to diverse materials. Polyhedral self-assembly occurs after patterned nets are released from the silicon substrate on which they are fabricated and heated above the melting point of the hinge material, which in the present case requires that the templates are heated in a high boiling point solvent (*N*-methylpyrrolidone) above the melting point of solder (183 °C). Assembly is driven by the minimization of surface tension of the liquid hinges both at the folding hinges which rotate the panels and at the locking hinges which self-align (26) and fuse the self-folding panels into place (Fig. 1 and Movie S1).

The use of liquid locking hinges at the edges of the panels is critical to enable self-assembly of higher order polyhedra with large numbers of panels, because they introduce favorable secondary interactions at the edges of the panels. As compared to solid mechanical latches utilized in earlier self-folding studies of optoelectronic structures on substrates (27), the introduction (28) of liquefiable locking hinges has lead to the facile assembly of polyhedra with high yields (9). The reason is that liquid locking hinges are deformable, and hence allow for small relative motions of the panels, thereby increasing fabrication defect tolerance. The small panel fluctuations are driven primarily by convective agitation of the solvent during heating. Our experimental methodology is also amenable to the use of alternate agitation schemes such as stirring or bubbling of an inert gas during heating. Because molten solder has a relatively high surface energy, large motions or complete separation of panels during assembly is rare. The angles between panels can be controlled by the volume of solder deposited, but panels are not programmed to fold in a particular sequence, nor are they actively controlled externally. When building polyhedra from nets, a prescription of folding rules is essential. Simple examples show that the same net may sometimes be folded into different polyhedra. Thus it is surprising that, in many of our experiments, nets self-fold with high yield into a specified 3D polyhedron.

Compactness as a Design Criterion. The nets were rarely varied in the first experiments on self-folding polyhedra. For example, a cruciform was almost always chosen to self-fold a cube. However, a recent study of the self-folding of all 11 nets for the cube and octahedron revealed that different nets fold through different pathways and have different yield (29). In particular, it was found that compact nets had higher yield. Both metric and topological measures of compactness were used. A metric measure of compactness is the radius of gyration, R_g, defined in Eq. **1** below. A topological measure of compactness, denoted V_c, is defined as follows. A vertex shared by two faces in the net that do not share an edge is called a vertex connection, and we say that the faces are topological neighbors. V_c is defined to be the total number of distinct vertex connections in a net. For example, the reader may count that nets in Fig. 2 *A–C* have $V_c = 2$, 6, and 10, respectively. These notions of compactness are correlated but distinct.

In this work, we test compactness as a design criterion for higher polyhedra, specifically the dodecahedron, icosahedron, and truncated octahedron. The number of nets for these polyhedra is too large for a complete experimental study. Instead, we computationally search the set of all nets, choose representative nets according to compactness, and test the selected nets for self-folding in experiments.

Summary of Results

We tabulated all 43,380 nets for the dodecahedron and icosahedron, and 123,452 nets (of 2.3 million estimated nets) for the truncated octahedron, using a Monte Carlo scheme. We then chose three nets for each polyhedron: the most compact, the least compact, and the median for each of the two compactness criterion. Several nets may have the same V_c, so when choosing nets according to V_c we made the following choice: Among all maximum V_c nets, we chose the net with smallest R_g; among all minimum V_c nets, we chose the net with highest R_g; and among all nets with the median V_c, we chose the net with median R_g. Fifty samples of each of these nets were self-folded experimentally and the resulting 3D structures were graded in three categories—A,

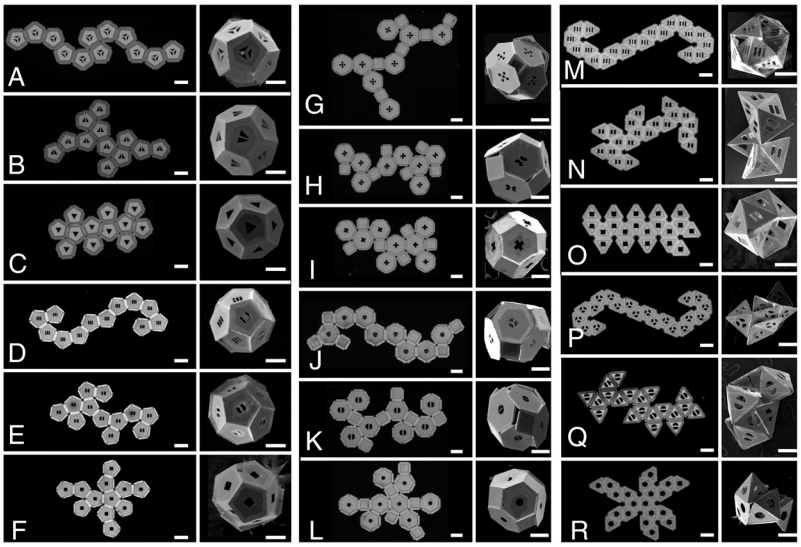

Fig. 2. Self-folding experiments on nets with varying V_c and R_g. Optical and SEM images showing photolithographically fabricated panels connected by solder hinges and the corresponding self-folded 3D structures respectively. (*A–F*) Dodecahedra in the order $V_c = 2$, 6, and 10, and $R_g = 1{,}102.2$, 800.9, and 693.7 μm, respectively. (*G–L*) Truncated octahedra in the order $V_c = 2$, 7, and 12, and $R_g = 1{,}306.3$, 912.7, and 795.0 μm, respectively. (*M–R*) Icosahedra in the order $V_c = 26$, 38, and 50, and $R_g = 711.1$, 514.6, and 445.4 μm, respectively. (Scale bar: 300 μm.)

B, and C—and the yield tabulated. "A" polyhedra were defect-free, "B" had minor defects, and "C" were defective. The experiments, grading scheme, and mathematics involved are described in greater detail in *Materials and Methods*.

Optical and SEM images showing the photolithographically fabricated 2D panels connected by solder hinges and representative self-folded 3D structures for all three polyhedra for both compactness criteria are shown in Fig. 2. Histograms of the yield are shown in Fig. 3. The yield is tabulated in Tables S1 and S2. We observe that both measures of compactness determine yield for these higher polyhedra just as for the cube and octahedron. Of the two measures, V_c is a better predictor. For the dodecahedron, the percentage of A-grade self-folded polyhedra from nets with the maximum V_c is more than five times that from nets with the lowest R_g, $R_g = 693.7$ μm. In addition, almost 80% of the maximum V_c samples are of grade A and B as compared with about 20% for the minimum R_g samples. For the truncated octahedron, the percentage of grade-A self-folded polyhedra from nets with the maximum V_c net is two times that of A-grade samples for minimum R_g, $R_g = 795$ μm. Moreover, almost 60% of the maximum V_c samples are of grade A and B as compared with about 30% for the minimum R_g samples. In contrast with these polyhedra, we were unable to fold any of the icosahedral nets. However, it is still the case that the more compact nets are less malformed than the others. Typical optical and SEM images for the icosahedron are shown in Fig. 2. SEM images of pathways are shown in Figs. S1 and S2.

There are 21 dodecahedron nets that have maximal V_c and we found four truncated octahedron nets that have maximal V_c (Fig. S3). As we have remarked above, the maximum V_c nets in Figs. 2 and 3 were chosen to have the lowest R_g among all nets with the same V_c. A finer investigation of maximum V_c nets was carried out in a second round of experiments. We repeated the self-folding experiments with 50 samples and the same grading scheme for four new dodecahedron nets (nets denoted 2, 5, 17, and 21 from Fig. S3*A*) and all four high V_c truncated octahedron nets (Fig. S3*B*). Images for these experiments are presented in Fig. 4 and histograms for the yield in Fig. 5. The yield is tabulated in Tables S3 and S4. We find again that the compact nets (as measured by low R_g now) have higher yield. We note that there is one common net (Fig. 2*I* and Fig. 4*H* for truncated octahedra). The yields of A-grade polyhedra from this net in two 50-sample experiments done months apart was 24% and 30%. This variation

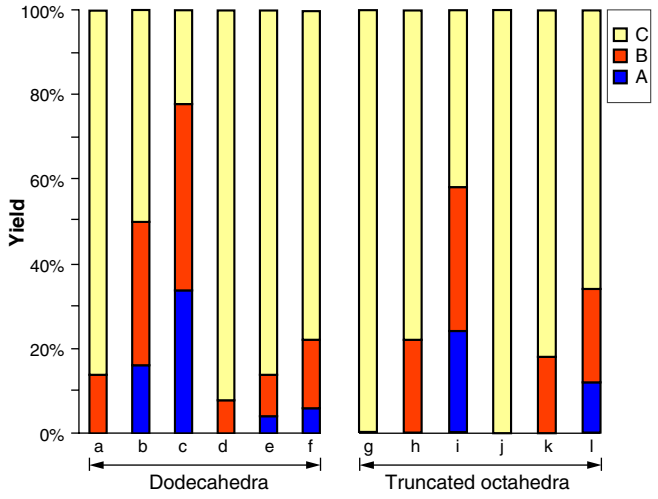

Fig. 3. Yield measured in self-folding experiments on nets with varying V_c and R_g. (*A–F*) Dodecahedral nets in the order $V_c = 2$, 6, and 10, and $R_g = 1{,}102.2$, 800.9, and 693.7 μm, respectively. (*G–L*) Truncated octahedral nets in the order $V_c = 2$, 7, and 12, and $R_g = 1{,}306.3$, 912.7, and 795.0 μm, respectively.

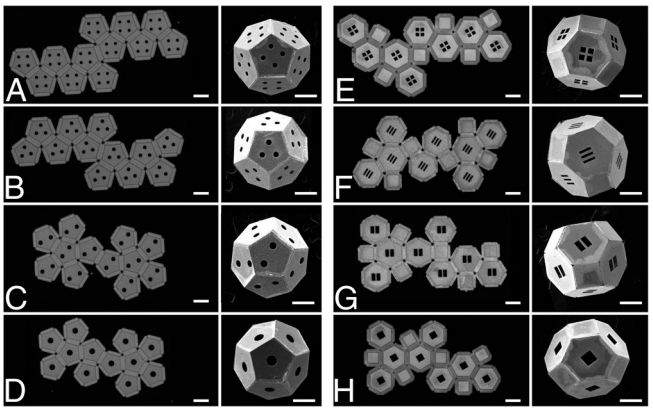

Fig. 4. Self-folding experiments on high V_c nets with varying R_g. Optical and SEM images. (*A–D*) Dodecahedral nets with $V_c = 10$ and $R_g = 810.2$, 797.4, 755.4, and 747.7 μm, respectively. (*E–H*) Truncated octahedral nets with $V_c = 12$ and $R_g = 911.6$, 870.2, 867.4, and 852.8 μm, respectively. (Scale bar: 300 μm.)

in the yield corresponds to a standard deviation of 4.2% in the plots of Figs. 3 and 5 and is consistent with the variation in our experiments.

Discussion

Algorithmic Design for Self-Assembly. We have found that the optimality criterion best suited to our experiments is to first maximize V_c and then minimize R_g. The superior performance of nets satisfying this criterion illustrates the importance of an algorithmic search. Of 123,452 truncated octahedron nets found, only four had $V_c = 12$. In contrast, the expected V_c for a random net chosen uniformly is approximately seven. Similarly, of the 43,380 dodecahedron nets, only 21 had $V_c = 10$ and the expected V_c is approximately six. For these polyhedra, Fig. 3 shows that the difference in yield between an optimal net and a uniformly chosen random net is dramatic.

Vertex Connections and Error-Correction. The effectiveness of compactness as a design criterion stems from its influence on the self-folding pathway. In experiments, we observe that topological compactness has two main consequences: (*i*) error correction at edges, and (*ii*) error correction in the pathway through partially rigid intermediates.

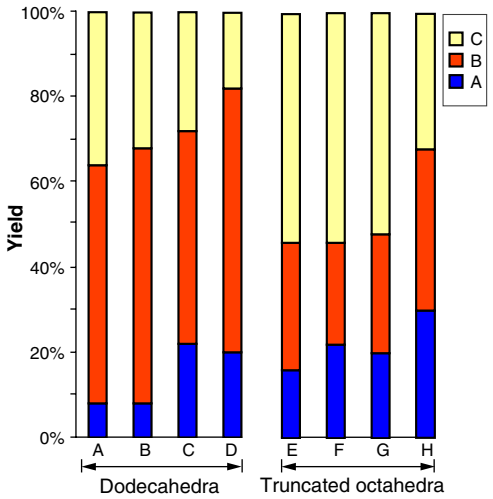

Fig. 5. Yield measured in self-folding experiments on high V_c nets with varying R_g. (*A–D*) Dodecahedral nets with $V_c = 10$ and $R_g = 810.2$, 797.4, 755.4, and 747.7 μm, respectively. (*E–H*) Truncated octahedral nets with $V_c = 12$ and $R_g = 911.6$, 870.2, 867.4, and 852.8 μm, respectively.

i. Outer panels are observed to fold before inner panels. When two outer panels are joined at a vertex connection, they begin by folding independently about their respective folding hinges. When the outer panels have folded by approximately the dihedral angle, the locking hinges meet and fuse. The liquid hinges then allow small readjustment so that the panels meet at the correct dihedral angles.

ii. Pathways that start with compact nets have intermediates that are more rigid. We say a mechanical linkage of panels is rigid if it cannot be deformed continuously while keeping each panel rigid. For example, a linkage of two square panels joined at a hinge is not rigid, but a linkage of three square panels joined at 90° at a corner is rigid. Dodecahedra and truncated octahedra that self-fold successfully from compact nets typically form rigid modules that mate with one another (Movie S1). Similar rigid intermediates are seen for the cube (29) (Fig. S2). In contrast, the pathway for the low V_c nets consists of more steps and involves the movement of long, floppy segments consisting of several panels (Fig. S1). Misalignment errors propagate during the motion of these segments. The absence of rigidity is a particular problem for the icosahedron. The icosahedron has 12 symmetric five-valent vertices and these must form as the net folds. Models of the pathways for the icosahedra show that even though high V_c nets eventually form symmetric halves that mate, neither these halves nor the intermediates that lead to them have rigid corners (Fig. S4). Intermediates have partially formed corners with three-, four-, or five-valent vertices. These corners are not rigid and can get misaligned as the net self-folds, even for the most compact nets.

Modeling Folding Pathways. In experiments, self-folding is a continuous transformation of a net into a polyhedron. However, it is useful to model self-folding as a discrete sequence of elementary steps, each of which corresponds to the gluing of locking hinges at vertex connections. First note that, to obtain a net from a convex polyhedron, we may cut it apart in a sequence of steps. At each step, we pick a face and cut along its edges until it is free to rotate and then rotate it to lie flat, as illustrated for the cube in Fig. 6*B*. In reverse, we may fold a net into a convex polyhedron by a process we call gluing at vertex connections: At each step, (*i*) a vertex connection on the boundary is chosen, and (*ii*) all faces linked by this vertex connection are glued at the locking hinges that meet at the chosen vertex connection. When gluing locking hinges, faces are only allowed to rotate rigidly through the dihedral angle about the folding hinges that meet at the vertex connection. If these rotations force other edges to meet, these are also glued. At each step of this process, new vertex connections may form, which may be used as new vertices for gluing. For all nets we consider, this procedure transforms the net into the polyhedron through a sequence of nonintersecting, partially folded intermediates (Fig. S4). We say that the discrete configuration space consists of all such intermediates, including the net and polyhedron.

The discrete configuration space is a graph. Each node in the graph corresponds to an intermediate, and its neighbors are intermediates to which it can be folded or unfolded. We define a distance between two intermediates in Eq. **1** below. This distance is defined using the geometric constraint that rotations about the folding hinges are required to fold or unfold one intermediate to another. Shortest paths between 2D nets and the 3D polyhedron are called geodesics.

The discrete configuration space and geodesics for the cube are illustrated in Fig. 7. An interesting feature is that the geodesics pass through only a small subset of the set of possible intermediates. For example, in row three of Fig. 7, we see that two dominant intermediates (states 1 and 5) "focus" the geodesics. State 5 consists of two rigid mating halves and three of the nets with maximum V_c (nets 2, 5, 9, with $V_c = 4$) fold through this intermediate. The configuration space of foldings is much larger

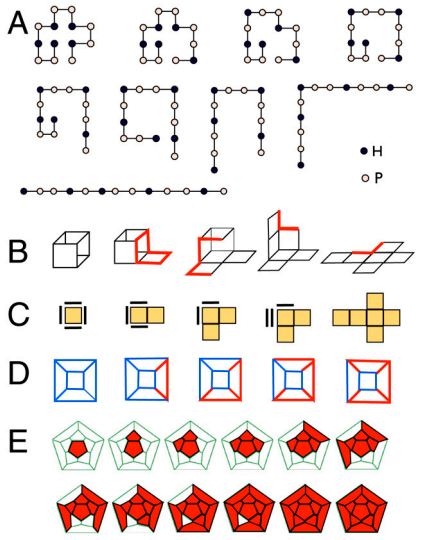

Fig. 6. Comparison of the discrete geometry of three self-assembly models. (*A*) Unfolding an HP chain. A compact HP chain on a 2D lattice is unfolded by breaking secondary HH bonds between topological neighbors. At each step, secondary bonds break and/or the chain reduces its discrete curvature. The compact configuration is chosen from ref. 31. The motion of the chain through kink jumps and rigid rotations is adapted from ref. 32. (*B–D*) Several representations of unfolding a cube. At each step, all edges linked at a vertex connection are cut so that a face is free to rotate rigidly through the dihedral angle, which gives faces linked through vertices but not edges (topological neighbors). (*B*) A perspective view. (*C*) A convenient schematic for the plan view that is used in Fig. 7. (*D*) Unfolding as two-color evolution on the graph of the cube: Cut edges are red and constitute a tree that grows at each step. Unfolding is complete when the tree is spanning. (*E*) Viral capsid assembly. Intermediate stages in the formation of a dodecahedral viral capsid following refs. 30 and 33. At each stage, a new face is added and congruent arrangements correspond to the same intermediate.

for the dodecahedron and truncated octahedron and cannot be represented as simply as Fig. 7. However, we have computed geodesics that originate at the nets chosen in our experiments. In particular, for the compact nets (Figs. 2 *C* and *F* and 4 *A–D* for the dodecahedron, and Figs. 2 *I* and *L* and 4 *E–H* for the truncated octahedron), we find that all computed geodesics pass through two dominant intermediates consisting of two mating half-dodecahedron or half-truncated octahedron (Fig. S4 *A* and *B*). These computed geodesic pathways may be compared visually with the experimentally observed folding pathways. When making this comparison, we focus on the later intermediates because, in the discrete model, folding occurs at one vertex at a time, whereas in experiments, outer panels can fold simultaneously. So it is only in the later stages that we can compare the model and experiment. In each case, we find that the dominant intermediates in the theoretically computed geodesics are typically also seen in experimentally observed pathways starting at the same net.

Some Common Themes in Self-Assembly. Our main objective in this work is algorithmic design to maximize yield and understand the pathways of self-folding. However, some central underlying questions arise in other mathematical models of self-assembly: What is the geometry of the configuration space of a self-assembling system? How can it be explored with experiment and computation? What are the pathways of assembly? Two examples that motivated us are compared with self-folding polyhedra in Fig. 6. A common feature shared by folding of HP chains on a lattice and self-folding a net through vertex connections is that in both cases the process of folding is driven by the formation of secondary links between topological neighbors. A common feature of self-folding pathways for nets and viral capsid assembly is that

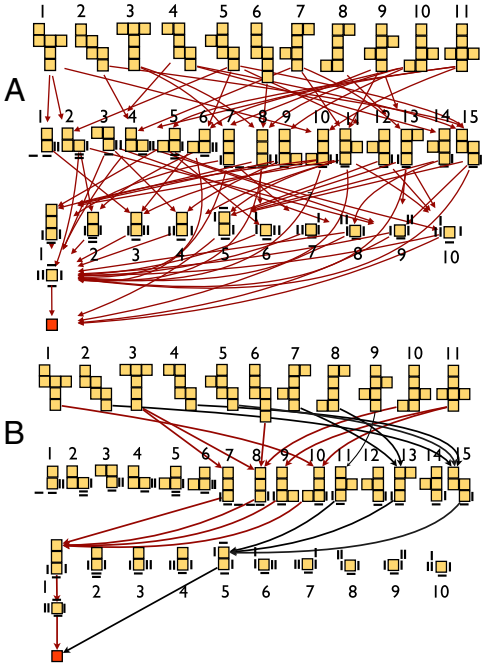

Fig. 7. (*A*) Computed configuration space and folding pathways for the cube. Partially folded intermediates and all folding pathways for the cube computed by the gluing at vertex connections algorithm. Multiplicity of edges connecting intermediates is not shown. Double bars denote vertically stacked faces. (*B*) Geodesics and dominant intermediates. Geodesic pathways between each net and the cube computed using Eq. **1**. The dominant intermediates are 1 and 5 in the third row. In this discrete model, nets 1, 3, 6, 10, and 11 fold through intermediate 1, and nets 2, 4, 5, 7, 8, and 9 fold through intermediate 5.

both can be modeled by similar evolutions of a two-color graph coloring on the polyhedron as explained in Fig. 6. In all three models, the configuration space is a graph and self-assembly may be modeled as a path on this graph between two special states: from the flat HP string, the net, and the empty polyhedral shell to an accessible compact string, the polyhedron, and the filled polyhedral shell. The structure of the configuration space is determined by an HP string (for the HP model) or polyhedron (for folding or capsid assembly). An explicit description (as in Fig. 7) is only possible in very small systems. The size of the configuration space explodes combinatorially as the length of the HP string grows or as the size of the polyhedron increases. A great deal of further computation on larger systems is necessary to establish whether the geometry of the configuration space in these examples shares some essential structure. The concentration of geodesics on a few dominant intermediates is a suggestive link; a similar collapse from all intermediates into a few dominant intermediates has also been observed for the assembly of viral capsids (30).

Conclusions

Our goal was to elucidate the geometric principles that underlie self-folding of polyhedron from nets. We have verified that compactness is an effective design criterion for several polyhedra by computationally exploring a large set of possible nets and testing selected nets experimentally. We also introduced a discrete configuration space of foldings and found that the geodesic between the 2D net and 3D polyhedron is a useful idealization of experimentally observed pathways.

These findings suggest further studies of self-folding in order to build more complex shapes and to minimize errors through the loss of rigidity. Although the number of nets is large for the polyhedra we considered, it was still amenable to an exhaustive search, which ceases to be the case for more complex polyhedra such as models for viral capsids. In seeking nets for realistic virus shapes, we have encountered polyhedra with approximately 10^{30} spanning trees (a number obtained from Kirchhoff's matrix tree theorem). It is impossible to find an optimal net and geodesics by an exhaustive search for such polyhedra, and suitable randomized algorithms must be used instead. On the experimental side, the ability to observe folding pathways provides additional insight into self-assembly. In combination, these techniques serve as a template for the emerging area of algorithmic design of self-assembly.

Materials and Methods

Experiments. Regular polyhedra were fabricated using a previously established process that enabled us to fabricate 3D polyhedra from 2D nets (24). Nets were chosen according to an algorithm described below. Fifty samples of each net were self-folded in the experiments. We used Autodesk AutoCAD to draw nets and then printed them on transparent sheets to make photomasks. Sides of a panel measured 300 μm, with two adjacent panels spaced apart by a width equal to 10% of the panel edge length. Optical lithography was used to develop features on a silicon wafer, and nickel and solder were electrodeposited on the panels and hinges, respectively. All V_c and R_g nets for a fixed polyhedron were processed across the same wafer with a uniform random distribution of nets to minimize processing variations during lithography. We released the nets from the substrate with nickel panels connected with solder hinges and heated the free-standing structures until they folded. All the nets for a fixed polyhedra were self-folded in close proximity in order to minimize the effect of variation in temperature and fluidic agitation. After self-folding, the solution was allowed to cool gradually. The molten solder solidified and the polyhedra were held robustly in place. Self-folded 3D structures realized from each net were carefully examined under an optical microscope and graded into three categories—A, B, and C. Grade-A polyhedra had no discernible defects when examined under an optical microscope. The dihedral angles were well formed (116.56° for dodecahedra, 125.27° for square and hexagonal panels of truncated octahedra, and 109.47° for two hexagonal panels of truncated octahedra). Grade-B polyhedra had the desired shapes but had faces that were misaligned with a maximum tolerance of 20° misalignment. Samples with defects more severe than 20° misalignment were graded as C polyhedra.

Mathematical Methods. Let Ω be a polygon in $\mathbb{R}^2$. The center of mass $(\bar{x}, \bar{y})$ and the radius of gyration R_g of Ω are given by the area integrals

$$(\bar{x},\bar{y}) = \int_\Omega (x,y)dA, \qquad R_g^2 = \int_\Omega (x-\bar{x})^2 + (y-\bar{y})^2 dA. \qquad [1]$$

We used a Monte Carlo scheme to generate random spanning trees and tabulate nets for each polyhedron. The main steps were as follows: (*i*) random spanning trees of the face-edge graph were found as follows. Independent weights uniformly distributed in (0,1) were assigned to the edges of the face-edge graph and a minimum weight spanning tree was found using either Kruskal's or Prim's algorithm. (*ii*) A traverse order of the spanning tree was chosen at random. A net was generated in this traverse order by linking each face with its connected neighbors using the face-edge graph. (*iii*) The planar boundary of the net was generated as a list of vertices. Because all edge lengths are equal here, the boundary was represented as a list of angles. Two such lists were compared to determine congruence (accounting for reflections and rotations). The main bottleneck in the algorithm is congruence testing. In practice, comparison of a list of angles is inefficient and hash tables were used. (*iv*) For the icosahedron and dodecahedron, the algorithm was run until all 43,380 nets had been found and we were satisfied that the algorithm did not generate any spurious nets. For the truncated octahedron, the algorithm was run until 123,452 nets had been found (an arbitrary number based on limitations on computer time). The Monte Carlo algorithm was also tested on the cube and octahedron and two smaller regular polyhedron (the pentagonal dipyramid and a square antiprism). These polyhedra have a smaller number of nets (98 and 231, respectively) intermediate between the cube (11) and the dodecahedron (43,380). The algorithm also yields a rough estimate of the total number of nets as follows: Let N denote the total number of nets, $r = 1 - 1/N$ and μ_n the expected number of nets found after step n. Under the assumption that all nets are equally likely, $\mu_n = N(1 - r^n)$ and this may be used to estimate N by linear regression. A posteriori we found that the assumption that all nets are equally likely in a trial is not valid, nevertheless the assumption was approximately valid, and the estimator

predicts accurate answers for the Platonic solids and dipyramid and antiprism. Based on this assumption, we estimate that the truncated octahedron has roughly 2.3 million nets.

When gluing at vertex connections, an intermediate is transformed to its neighbors through a sequence of rotations about folding hinges that meet at the vertex connection. For example, to transform intermediate 11, row 1 to intermediate 10, row 2 in Fig. 7*A*, we must rotate two panels one after the other by 90°. More formally, an intermediate I is folded into a neighbor J through a chain of states $(S_0,S_1,\ldots,S_k)$, $S_0 = I$, $S_k = J$ each of which differ by a single rotation about a folding hinge. We first define the distance between two states S_j and S_{j+1} as follows. Assume S_j is transformed to S_{j+1} by a rotation about a folding hinge through an angle θ. The folding hinge separates the starting configuration S_j into two connected domains denoted Ω_1 and Ω_2. If the domain Ω_i rotates through an angle θ_i about the folding hinge, each point in Ω_i at a distance r from the axis travels on a circular arc of length $r\theta_i$. The total squared distance traveled by Ω_i is then $\int_{\Omega_i}(r\theta_i)^2 dA = I_i\theta_i^2$, where I_i is the second moment of area of the domain Ω_i about the folding hinge. We minimize the total distance $I_1\theta_1^2 + I_1\theta_2^2$ subject to the constraint $\theta_1 + \theta_2 = \theta$ to obtain $d^2(S_j,S_{j+1}) = (I_1I_2/(I_1 + I_2))\theta^2$. The distance between two intermediates I and J in the configuration space is then defined to be

$$d^2(I,J) = \min \sum_{j=0}^{k-1} d^2(S_j,S_{j+1}), \qquad [2]$$

where the minimum is taken over all sequences of admissible rotations $(S_0,S_1,\ldots,S_k)$, $S_0 = I$, $S_k = J$ that transform I into J.

ACKNOWLEDGMENTS. This work was supported by National Science Foundation Grants Division of Mathematical Sciences 0748482, Emerging Frontiers in Research and Innovation (EFRI) 1022638, and EFRI 1022730.

1. Whitesides G, Grzybowski B (2002) Self-assembly at all scales. *Science* 295:2418–2421.
2. Caspar D, Klug A (1962) Physical principles in the construction of regular viruses. *Cold Spring Harb Symp Quant Biol* 27:1–24.
3. Lau K, Dill K (1989) A lattice statistical mechanics model of the conformational and sequence spaces of proteins. *Macromolecules* 22:3986–3997.
4. Chan H, Dill K (1990) The effects of internal constraints on the configurations of chain molecules. *J Chem Phys* 92:3118–3135.
5. Chen J, Seeman N (1991) Synthesis from DNA of a molecule with the connectivity of a cube. *Nature* 350:631–633.
6. He Y, et al. (2008) Hierarchical self-assembly of DNA into symmetric supramolecular polyhedra. *Nature* 452:198–201.
7. Zimmermann J, Cebulla M, Mönninghoff S, von Kiedrowski G (2008) Self-assembly of a DNA dodecahedron from 20 trisoligonucleotides with c3h linkers. *Angew Chem Int Ed Engl* 47:3626–3630.
8. Douglas S, et al. (2009) Self-assembly of DNA into nanoscale three-dimensional shapes. *Nature* 459:414–418.
9. Leong T, Zarafshar A, Gracias D (2010) Three-dimensional fabrication at small size scales. *Small* 6:792–806.
10. Boncheva M, Gracias D, Jacobs H, Whitesides G (2002) Biomimetic self-assembly of a functional asymmetrical electronic device. *Proc Natl Acad Sci USA* 99:4937–4940.
11. Mahadevan L, Rica S (2005) Self-organized origami. *Science* 307:1740.
12. Rechtsman M, Stillinger F, Torquato S (2006) Designed interaction potentials via inverse methods for self-assembly. *Phys Rev E Stat Nonlin Soft Matter Phys* 73:011406.
13. Cohn H, Kumar A (2009) Algorithmic design of self-assembling structures. *Proc Natl Acad Sci USA* 106:9570–9575.
14. Bassik N, Stern G, Gracias D (2009) Microassembly based on hands free origami with bidirectional curvature. *Appl Phys Lett* 95:091901.
15. Barish R, Schulman R, Rothemund P, Winfree E (2009) An information-bearing seed for nucleating algorithmic self-assembly. *Proc Natl Acad Sci USA* 106:6054–6059.
16. Hormoz S, Brenner M (2011) Design principles for self-assembly with short-range interactions. *Proc Natl Acad Sci USA* 108:5193–5198.
17. Demaine E, O'Rourke J (2007) *Geometric Folding Algorithms. Linkages, Origami, Polyhedra* (Cambridge Univ Press, New York), pp 299–338.
18. Dürer A, Strauss W (1977) *The Painter's Manual* (Abaris, New York) p 433.
19. Cromwell P (1999) *Polyhedra* (Cambridge Univ Press, Cambridge, UK), pp 126–127.
20. Wenninger M (1974) *Polyhedron Models* (Cambridge Univ Press).
21. Shephard G (1975) Convex polytopes with convex nets. *Math Proc Cambridge Philos Soc* 78:389–403.
22. Buekenhout F, Parker M (1998) The number of nets of the regular convex polytopes in dimension 4. *Discrete Math* 186:69–94.
23. Horiyama T, Shoji W (2011) Edge unfoldings of Platonic solids never overlap. *Proc 23rd Canadian Conf Computational Geom (CCCG2011)*, www.2011.cccg.ca.
24. Leong T, Lester P, Koh T, Emma K, Gracias D (2007) Surface tension-driven self-folding polyhedra. *Langmuir* 23:8747–8751.
25. Azam A, Laflin K, Jamal M, Fernandes R, Gracias D (2011) Self-folding micropatterned polymeric containers. *Biomed Microdevices* 1–8.
26. Wale M, Edge C, Randle F, Pedder D (1989) A new self-aligned technique for the assembly of integrated optical devices with optical fibre and electrical interfaces. *Proceedings of the 15th European Conference on Optical Communications (ECOC)* (Novum Grafiska AB, Stockholm), pp 368–371.
27. Syms R (1999) Surface tension powered self-assembly of 3-D micro-optomechanical structures. *J Microelectromech Syst* 8:448–455.
28. Gimi B, et al. (2005) Self-assembled three dimensional radio frequency (RF) shielded containers for cell encapsulation. *Biomed Microdevices* 7:341–345.
29. Azam A, Leong T, Zarafshar A, Gracias D (2009) Compactness determines the success of cube and octahedron self-assembly. *PloS One* 4:e4451.
30. Endres D, Miyahara M, Moisant P, Zlotnick A (2009) A reaction landscape identifies the intermediates critical for self-assembly of virus capsids and other polyhedral structures. *Prot Sci* 14:1518–1525.
31. Dill K, Chan H (1997) From Levinthal to pathways to funnels. *Nat Struct Biol* 4:10–19.
32. Verdier P, Stockmayer W (1962) Monte Carlo calculations on the dynamics of polymers in dilute solution. *J Chem Phys* 36:227–235.
33. Wales D (1987) Closed-shell structures and the building game. *Chem Phys Lett* 141:478–484.

Supporting Information

Pandey et al. 10.1073/pnas.1110857108

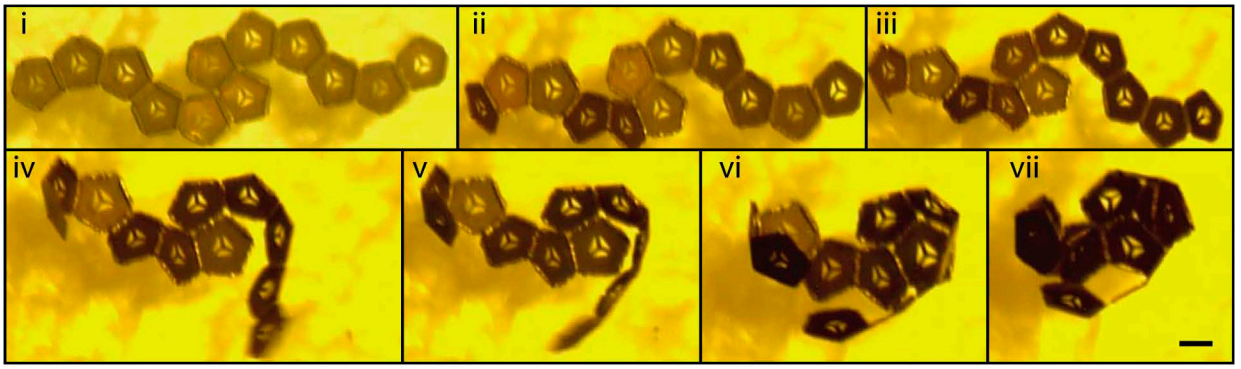

Fig. S1. Folding pathway for the dodecahedron (V_c). Optical microscopy images showing a folding pathway of a dodecahedral net with $V_c = 2$ as in Fig. 2*A*.

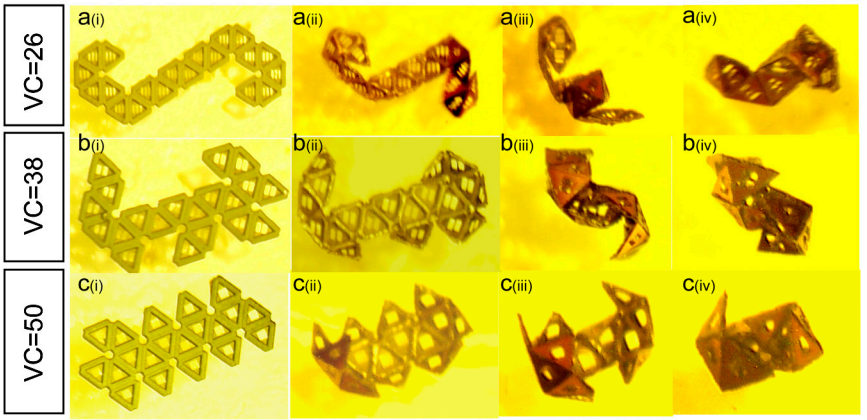

Fig. S2. Folding pathways for the icosahedron. Optical microscopy images showing folding pathways of icosahedral nets with 3D structure for the icosahedron. *A i–iv*, $V_c = 26$; *Bi–iv*, $V_c = 38$; *C i–iv*, $V_c = 50$.

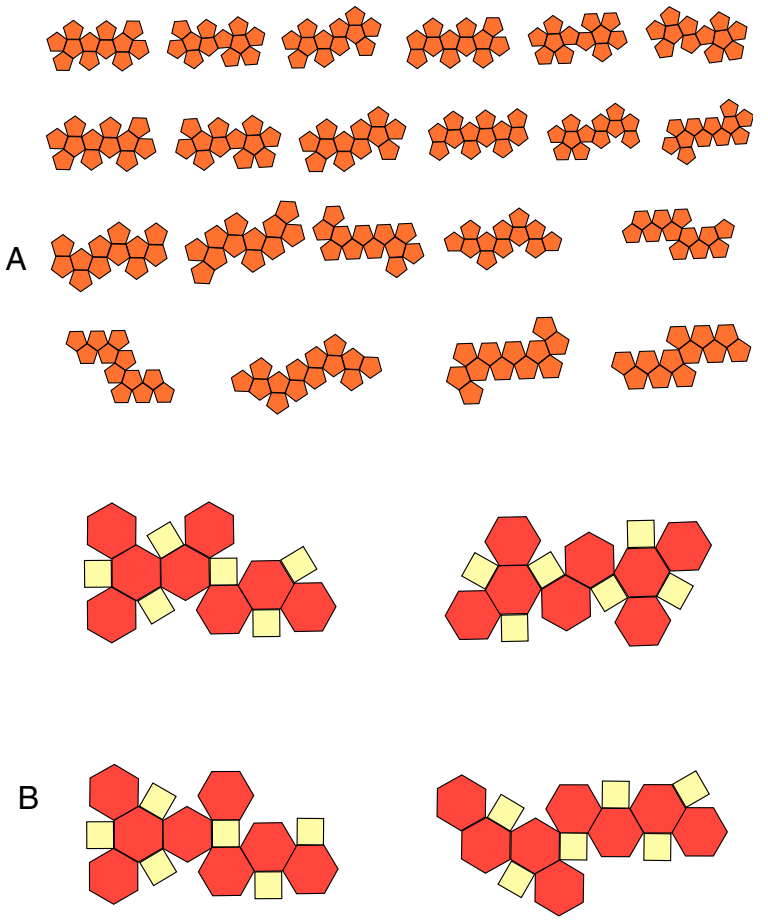

Fig. S3. (*A*) High V_c nets for the dodecahedron. All $V_c = 10$ nets (21 out of all 43,380) arranged in order of increasing R_g; (*B*) High V_c nets for the truncated octahedron. All $V_c = 4$ nets (four out of the 123,452 nets found) are shown.

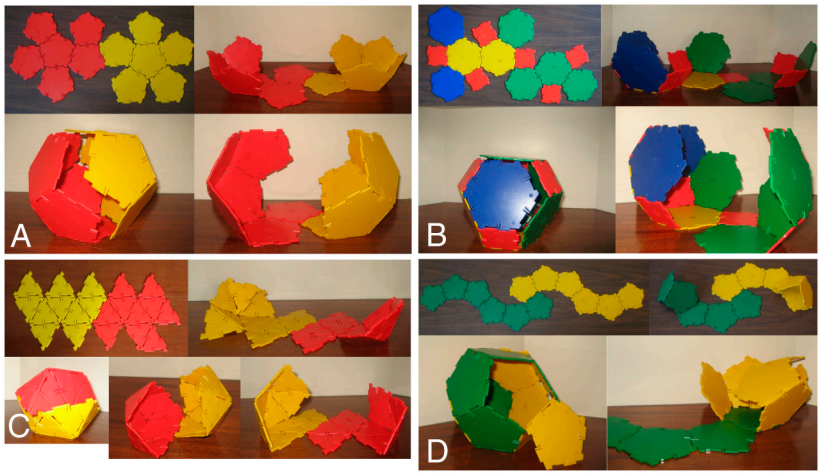

Fig. S4. Models illustrating the gluing at vertex connections algorithm. Manually folded centimeter-scale models. (*A*) $V_c = 10$ dodecahedron; (*B*) $V_c = 12$ truncated octahedron; (*C*) $V_c = 50$ icosahedron; (*D*) $V_c = 2$ dodecahedron. *A*–*C* are high V_c nets. They have the common feature that the penultimate intermediate consists of two mating halves. The same intermediates are also see in experiments with these nets for the dodecahedron and truncated octahedron and also in computed geodesics. However, these halves are rigid only for *A* and *B*. Both *C* and *D* are not rigid. The five-valent vertices in *C*, though fully formed, are not rigid. *D* has long floppy segments that lead to misaligned structures. Surprisingly, it does yield some "B-grade" specimens (see Figs. 2 and 4).

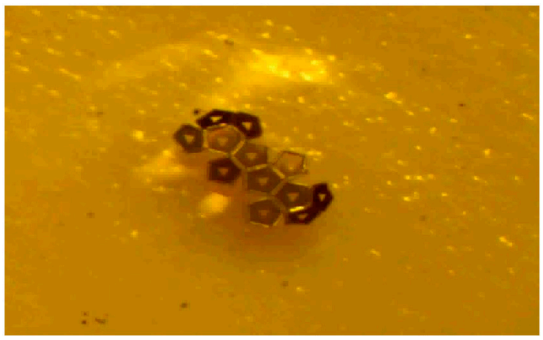

Movie S1. Folding pathway for the dodecahedron ($V_c = 10$). Optical microscopy movie of self-folding for a dodecahedral net with $V_c = 10$ as in Fig 2C.

Movie S1 (WMV)

Table S1. Yields for all 300-μm dodecahedron nets

Net	%A	%B	%C
$V_c = 2$	0	14	86
$V_c = 6$	16	34	50
$V_c = 10$	34	44	22
$R_g = 1{,}102.2$ μm	0	8	92
$R_g = 800.9$ μm	4	10	86
$R_g = 693.7$ μm	6	16	78

Fifty samples were tested for each net.

Table S2. Yields for all 300-μm truncated octahedron nets

Net	%A	%B	%C
$V_c = 2$	0	0	100
$V_c = 7$	0	22	78
$V_c = 12$	24	34	42
$R_g = 1{,}306.3$ μm	0	0	100
$R_g = 912.7$ μm	0	18	82
$R_g = 795.0$ μm	12	22	66

Fifty samples were tested for each net.

Table S3. Yields of 300-μm dodecahedron nets with same number of vertex connections ($V_c = 10$) and different radius of gyration (R_g)

Net, μm	%A	%B	%C
$R_g = 810.2$	8	56	36
$R_g = 797.4$	8	60	32
$R_g = 755.4$	22	50	28
$R_g = 747.7$	20	62	18

Table S4. Yields of 300-μm truncated octahedron nets with same number of vertex connections ($V_c = 12$) and different radius of gyration (R_g)

Net, μm	%A	%B	%C
$R_g = 911.6$	16	30	54
$R_g = 870.2$	22	24	54
$R_g = 867.4$	20	28	52
$R_g = 852.8$	30	38	32